JOURNAL OF MATERIALS SCIENCE 37 (2002) 2367–2375

Layered $LiNi_{1-y}Co_yO_2$ compounds synthesized by a glycine-assisted combustion method for lithium batteries

C. JULIEN, C. LETRANCHANT, M. LEMAL, S. ZIOLKIEWICZ
Laboratoire des Milieux Désordonnés et Hétérogènes, UMR7603, Université Pierre et Marie Curie, 4 place Jussieu, 75252 Paris cedex 05, France
E-mail: cjul@ccr.jussieu.fr

S. CASTRO-GARCIA
Departamento Quimica Fundamental e Industrial, Universidade A Coruna 15071 A Coruna, Spain

The lithiated nickel-cobalt oxide cathode materials were prepared at low temperature using the aqueous glycine-nitrate combustion method. Physicochemical and electrochemical properties of $LiNi_{1-y}Co_yO_2$ ($0.3 \leq y \leq 0.7$) calcined at 400–600°C were extensively investigated. It has been found that powders of submicron-sized particles with a layered structure ($R\bar{3}m$ space group) were obtained at temperatures below 400°C by the acidification reaction of the aqueous nitrate solution. The method involves the mixing of nitrates of Li, Ni and Co, with a combustion agent, glycine in an aqueous medium. Glycine functioned such as a fuel, decomposed the homogeneous precipitate of metal complexes at low temperature, and yielded the free impurity $LiNi_{1-y}Co_yO_2$ compounds. The synthesized products were characterized by structural (XRD, SEM), spectroscopic (FTIR) and thermal (DTA/TG) analyses. The electrochemical properties of the synthesized products in rechargeable Li cells were evaluated using a non-aqueous organic electrolyte mixture of 1 *M* $LiPF_6$ in EC + DMC. The electrodes fired at low temperature exhibed a good cycling behavior. © *2002 Kluwer Academic Publishers*

1. Introduction

Lithiated transition-metal oxides with a layered, α-$NaFeO_2$-type, structure such as $LiMO_2$ (M = Ni and Co) have been extensively studied this last decade such as positive electrode materials for rechargeable lithium batteries. $LiCoO_2$ has been proposed as cathode for lithium battery by Mizushima *et al.* in 1980 [1]. The concept of Li-ion cell has been demonstrated on either in D-, AA-, or coin-sized cells based on $LiCoO_2$/electrolyte/carbon, $LiNiO_2$/electrolyte/carbon, and $LiNi_{0.2}Co_{0.8}O_2$/electrolyte/carbon electrochemical chains, respectively [2–4]. A number of commercial lithium-ion batteries (e.g., from Sony, Panasonic, Sanyo, and SAFT) using different anode and cathode materials are currently being produced for consumer products.

Layered lithium transition-metal oxides (LTMOs) such as lithium cobaltate and lithium nickelate are the most advanced studied electrode materials. Their use in rechargeable Li-ion batteries shows some limitations due to its expensive technology, toxicity, cycle life failure, and coexistence of two phases are a debatable subject in using $LiCoO_2$ [5]. Lithium nickelate, $LiNiO_2$, is one of the most attractive materials for lithium-ion cells, but hard to prepare in a reproducible way due to the tendency to non-stoichiometric growth, and strong activity in the electrochemically formation of nickel dioxide at low lithium content which induces an organic electrolyte oxidation and an exothermic reaction. Voltages in excess of 4 volts occur for low lithium contents making LTMO cathodes highly oxidizing and, therefore, unstable in many of the organic-based electrolytes that are utilized in lithium cells [6, 7]. To alleviate the above disadvantages, many attempts have been made to improve the lithium insertion-deinsertion properties of both $LiCoO_2$ and $LiNiO_2$ by partial substitution of Co or Ni. The most well-documented approach is the solid solution $LiNi_{1-y}Co_yO_2$ series [8–13]. $LiNi_{1-y}Co_yO_2$ compounds are isostructural with the layered oxide end-compounds. They exhibit electrochemical features with lower insertion potentials compared to that for the pure cobalt oxide phase, $LiCoO_2$. Therefore, $LiNi_{1-y}Co_yO_2$ compounds were expected to be oxidatively less demanding on the electrolyte phase and to exhibit good lamellar structure. With increasing cobalt content, the trigonal distortion of the crystal lattice increases and the deviation from the stoichiometry of lithium nickelate decreases.

In recent years, there has been a great deal of interest in preparation of polycrystalline materials, particularly oxides, using low-temperature (LT) techniques. Low-temperature crystallized lithiated

transition-metal oxides (LT-LTMOs), which showed some promise in improving the cycle life of rechargeable lithium batteries, have been grown by new synthesis routes such as sol-gel, combustion, and precipitation methods using complexing agents like succinic, oxalic, malic or tartaric acids [14–18]. Recently, Pereira-Ramos has critically discussed the impact afforded by LT techniques especially sol-gel synthesis and precipitation techniques on the electrochemical behavior of the oxide materials as prepared [19]. Solution preparative techniques allow a better mixing of the elements and thus a better reactivity of the mixture to obtain purer reaction products. Lower reaction temperature and shorter reaction time are then possible to yield a compound of high homogeneity and high specific area. Moreover, these LT methods make use of lower calcination temperatures resulting in particles of smaller size and a highly uniform morphology of crystallized materials which are desired parameters with low strained lattice [20–22].

The present work has been aimed at carrying out systematic investigations on $LiNi_{1-y}Co_yO_2$ ($0.3 \leq y \leq 0.5$) electrode materials synthesized by a new procedure, namely the aqueous glycine-nitrate combustion method. The combustion method consists in an acidification reaction using an organic (carboxylic-type) acid. The complexing agent acts such as a fuel during the formation process of LTMO powders. The carboxylic acid groups present in the complexing agent could form a chemical bond with the metal ions and forms viscous resins on evaporation of the solvent, which are usually called as precursors. In this paper, physical and electrochemical of properties of $LiNi_{1-y}Co_yO_2$ synthesized by the glycine-assisted method are reported for the first time. Physical studies were carried out by different techniques like XRD, FTIR, DTA, and SEM. The LT procedure provides microcrystalline, layered $LiNi_{1-y}Co_yO_2$ compounds with uniform submicron-sized particles. The FTIR results should give useful information on the local structure of materials. The electrochemical performance of these oxides has been studied by coupling them as cathodes with Li anodes and a non-aqueous electrolyte mixture.

2. Experimental

2.1. Sample preparation

The $LiNi_{1-y}Co_yO_2$ samples were grown using a wet-chemical synthesis at low-temperature, namely glycine-nitrate combustion (pyrolysis) method. The flow chart showing the steps used in the processing of lithium-nickel-cobalt oxide powders is presented in Fig. 1. The LTOMs were grown from acetates via inorganic polymerization reactions in acidic solution. Compared with the conventional powder route, it is believed that this technique offers many advantages such as a lower temperature processing and better control of morphology of materials.

A stoichiometric amount of lithium and metal nitrate salts was dissolved in triple distilled water with a small proportion of ethanol and mixed with an aqueous solution of glycine (aminoacetic acid, NH_2CH_2COOH). In this case, care was exercised in adjusting the concentration of the complexing agent, the pH of the solution ranges between 2–3. Then, this acidic solution was evaporated to dryness at 80°C for few hours. The rose-red colour solution turned to violet colour product which decomposed by heating at 120°C to give a brownish black powder (precursor). The slurries were heated at 400°C for few hours to get the product of the composition $LiNi_{1-y}Co_yO_2$. Glycine acts as a fuel, decomposes the homogeneous precipitate of metal complexes at low temperature, and yields the free impurity $LiNi_{0.3}Co_{0.7}O_2$ compound. During this process the $LiNi_{1-y}Co_yO_2$ mass precursor darkened progressively as a result of oxidation. The origin of the colour change during the firing process is obviously due to oxidation of divalent cations (Ni^{2+}, Co^{2+}) to trivalent cations (Ni^{3+}, Co^{3+}). It is a fine grained material of submicrometer size and the yield is a brownish-black powder. Accordingly, the powder mass was slightly ground and then fired at 600°C in air for 5 h to improve the crystallinity $LiNi_{1-y}Co_yO_2$ final product. A theoretical reaction, assuming complete thermal decomposition of the starting materials, may be written as

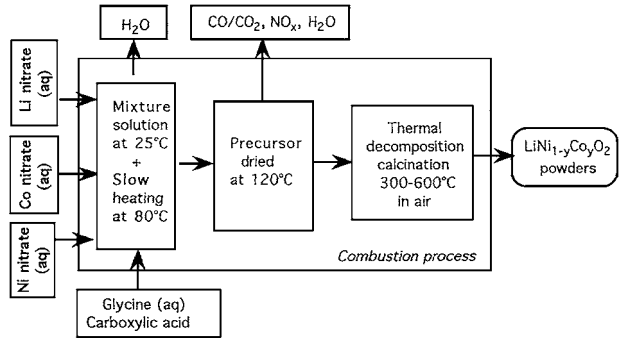

Figure 1 Synthetic procedure of polycrystalline $LiNi_{1-y}Co_yO_2$ powders by wet-chemical technique via the glycine-assisted combustion method.

$$\begin{aligned} &LiNiO_3(aq) + (1-y)Ni(NO_3)_2(aq) + yCo(NO_3)_2 \\ &\quad + 6NH_2CH_2COOH(aq)\Delta\text{in air} \\ &\quad \rightarrow LiNi_{1-y}Co_yO_2(s) + 2N_2(g) \\ &\quad + 2CO_2(g) + 2CO(g) + 3H_2O(g), \end{aligned} \tag{1}$$

which ultimately gave rise to a brownish black powder.

Powders were first studied by several physical characterization techniques, such as thermal analysis, powder x-ray diffraction (XRD), Fourier transform infrared (FTIR) spectroscopy and scanning electron microscopy (SEM).

2.2. Instruments

The thermal decomposition behavior of the precursor was examined by means of thermogravimetry (TG) and differential thermal analysis (DTA) using a Netzsch analyser (model STA 409) with the simultaneous recording of weight losses (gravimetric thermal analysis) and temperature variations (differential scanning calorimetry). X-ray diffraction patterns were obtained with a Philips x-ray diffractometer (model PW1830) using nickel-filtered Cu K_α radiation ($\lambda = 1.5406$ Å).

The diffraction patterns were taken at room temperature in the range of $10^\circ < 2\theta < 80^\circ$ using step scans. The step size and the scan rate were set at 0.1 and 0.2 degree/min, respectively. The particle morphologies of the materials were examined by scanning electron microscopy (SEM, Cambridge Instruments, Stereoscan 120). FTIR absorption spectra were recorded at room temperature using an interferometer (Bruker model IFS113v) equipped with a 3.5 μm-thick beamsplitter, a globar source, and a DTGS/PE far-infrared detector. Samples were ground to fine powders painted onto pellets of solid paraffin or polyethylene slabs. Data were collected in transmission mode at a spectral resolution of 2 cm^{-1} after 256 scans in vacuum atmosphere.

Electrochemical studies were carried out on the synthesized products annealed at 600°C in order to test their suitability as cathode-active materials in high voltage lithium-containing batteries. The laboratory-scale Li//$LiNi_{1-y}Co_yO_2$ cells were fabricated employing a non-aqueous electrolyte prepared by dissolving 1*M* $LiPF_6$ in 1 : 1 (v/v) mixture of ethylene carbonate (EC) and dimethyl carbonate (DMC), respectively. The typical composite cathodes consisted of the mixture of active $LiNi_{1-y}Co_yO_2$ powders, acetylene black, and colloidal PTFE binder in the 90 : 5 : 5 weight ratio. The PTFE-acetylene black was used to provide good electrical conductivity as well as mechanical toughness between active grains. The above mixture was pressed on to an expanded aluminium microgrid at a pressure of 500 MPa. This procedure yielded circular pellet electrodes of 10 mm diameter. The pellets were then dried at 120°C in air. Whatman glass fiber membrane was used as the separator between the cathode and the anode [23]. Electrodes and separators were soaked in the electrolyte before being housed in a Teflon laboratory-cell hardware. In order to assess their electrochemical performance, galvanostatic charge-discharge cycles were recorded using a Mac-Pile system at a slow scan mode (i.e. current pulse of 0.1 mA/cm^2 for 1 h followed by relaxation period of 0.5 h) in the potential range between 2.5 and 4.0 V.

3. Results and discussion

3.1. Thermal analysis

Fig. 2 shows the TG-DTA curves which display the formation temperature of the oxide $LiNi_{1-y}Co_yO_2$ grown by the glycine-assisted combustion method. A strong exothermic peak appears in the range 230–250°C after the departure of the remaining water molecule at ca. 120°C. The formation temperature of the oxide prepared from the combustion-method precursor occurs at the low temperature of 217°C for $y = 0.7$. The exothermic effect corresponds to the combustion of glycine-nitrates. More than half of the weight loss occurs during this stage because of a violent oxidation-decomposition reaction. During the combustion process, the rose-red solution turned into violet-colour gel then burnt to give brownish black powder. Assuming that glycine provides combustion heat for calcination in the synthesis of oxide powders, it appeared that this aminoacetic acid acts as a fuel during the pyrolysis of the precursor, accelerating the decomposition of nitrate ions in the process. Eventhough the crystallisation starts below 400°C; thus well-crystallized and pure phases have been obtained at 600°C. While the pyrolysis at this stage was very complicated, it could be presumed that the last weak exothermic at ca. 380°C in the DTA curves corresponds to the crystallization of $LiNi_{1-y}Co_yO_2$ phase.

3.2. Structure and morphology

X-ray diffraction analysis was carried out on the synthesized products at various preparation stages of $LiNi_{1-y}Co_yO_2$ powders to monitor the phase purity and structure, phase concentrations and the amorphous content. These preliminary results obtained from the precursors are indicating that polycrystalline powders are grown with the tendency of a layered α-$NaFeO_2$-type structure. When a material was precalcined at 400°C, a significant amount of the $LiNi_{1-y}Co_yO_2$ phase peaks and a small amount of the impurity peaks are detected. This is quite consistent with the DTA data which show the crystallization peak at 380–398°C.

Fig. 3 shows the x-ray diffraction patterns of microcrystalline $LiNi_{1-y}Co_yO_2$ powders (with $0.3 \leq y \leq 0.7$) grown by the glycine-assisted combustion method. Single-phase materials with an α-$NaFeO_2$-type structure was grown when the precursors were calcined at 600°C. It took at least 5 h to attain full crystallinity. XRD peaks were indexed in the hexagonal system assuming the $R\bar{3}m$ symmetry. It is assumed that lithium ions are in octahedral sites between $(Ni_{1-y}Co_yO_2)_n$ infinite slabs formed by edge-sharing $(Ni_{1-y}Co_y)O_2$ octahedra. Hexagonal cell parameters of the oxides prepared by different cobalt concentrations were calculated by least-squares refinement. They are given in Table I. These results are in good agreement with values reported in the literature [9]. Both the metal-metal intrasheet distance (a_{hex}) and the metal-metal interlayer distance ($c_{hex}/3$) decrease with increasing cobalt

TABLE I XRD results obtained on $LiNi_{1-y}Co_yO_2$ powders calcined at 600°C. The lattice parameters are given assuming the $R\bar{3}m$ symmetry (hex.)

	Lattice parameters				Fitting parameters	
Cobalt content	a (Å)	c (Å)	c/a	V(Å^3)	R-value[a]	Q-value[b]
0.3	2.850	14.128	4.957	99.38	0.023	0.74
0.5	2.841	14.113	4.967	98.66	0.012	0.66
0.7	2.832	14.080	4.972	97.79	0.153	0.78

[a] Calculated from $R = \Sigma|I\text{obs-}I\text{cal}|/\Sigma|I\text{obs}|$.
[b] Calculated from the x-ray intensity of $I(104)/I(003)$.

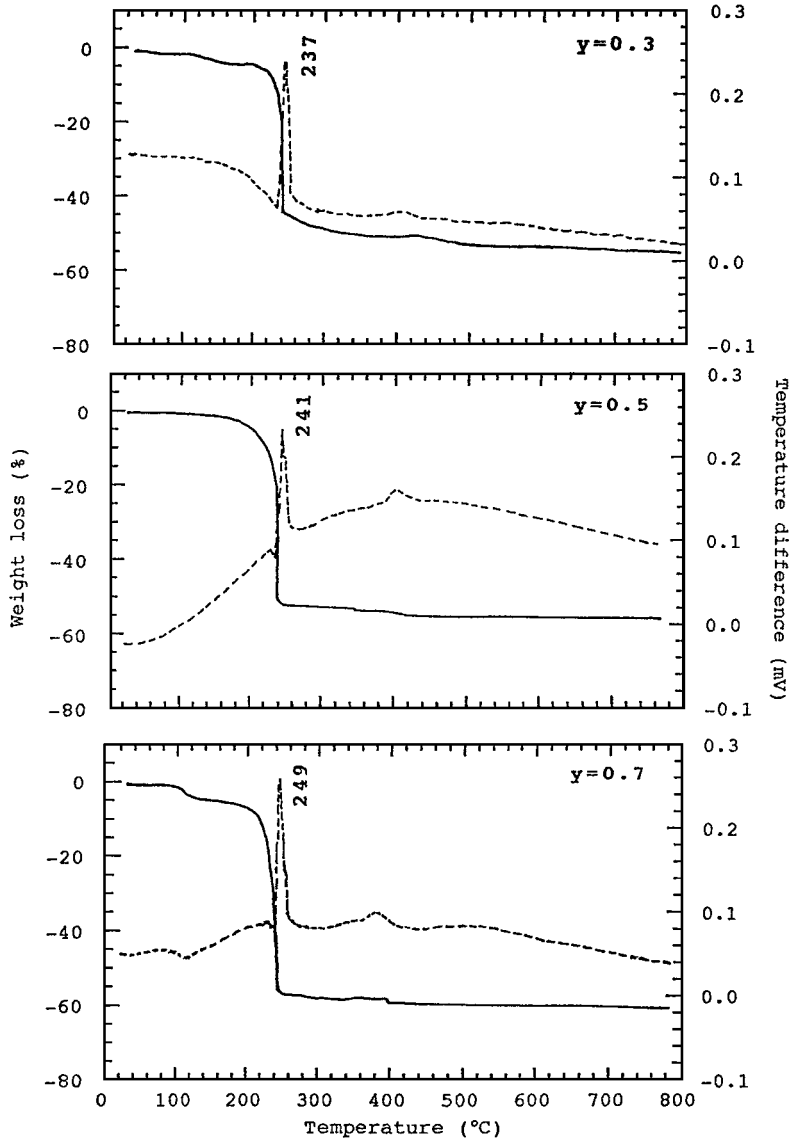

Figure 2 TG-DTA curves of the $LiNi_{1-y}Co_yO_2$ ($0.3 \leq y \leq 0.7$) grown by the glycine-assisted combustion technique. These measurements were carried out at a heating rate of 10°C/min with oxygen flow. Full lines correspond to the gravimetric thermal curves and dashed lines represent the differential scanning calorimetry curves.

concentration (Table I). Constructing the crystallographic $Ni_{1-y}Co_yO_2$ layers by substituting the sites of the Co^{3+} ions for the Ni^{3+} ions and calculating correspondingly the c/a value (~4.96), one reveals that the hexagonal-close-packed lattice is still maintained, in other words, no cation mixing between the Ni^{3+} and Li^+ ions present in octahedral sites if the c/a value is significantly larger than 4.90. As indicated by XRD data the sample particles are submicron-sized spherical grains in oxides prepared by the wet-chemical method. Cobalt-rich compounds ($y \geq 0.5$) grown by combustion method exhibit XRD patterns with well-defined (006,102) and (108,110) doublets. The c/a ratio (Table I) very different from the critical value 4.90 and the clear splitting of the (006) and (102) as well as (108) and (110) diffraction lines indicate that, as far as XRD patterns are concerned, an ordered distribution of lithium and transition-metal ions exists in the structure [24, 25]. On the other hand, the XRD diagram of nickel-rich materials (Fig. 3) exhibits peaks due to impurities and Bragg doublets poorly defined. XRD results confirm the single-phase formation of cobalt-rich cathode materials, but the question of the local cationic order will be re-examined below by spectroscopic measurements.

Surface morphology and texture as well as particle sizes were observed by scanning electron microscopy. Fig. 4a–b shows typical SEM micrographs of $LiNi_{0.3}Co_{0.7}O_2$ and $LiNi_{0.5}Co_{0.5}O_2$ samples annealed at 600°C. The powders observed by SEM were found to be submicron-sized particles, i.e. the grain size average is about 800 nm. The crystallite sizes tended to increase as the sintering time increased, and ranged in size from 800 to 1000 nm, suggesting the formation of micron-sized particles with a narrow grain size distribution.

3.3. Vibrational spectra

The purpose of this study is to investigate the local environment of cations in a cubic close-packed oxygen array of the $LiNi_{1-y}Co_yO_2$ lattice using FTIR spectroscopy. IR modes correspond to vibrations involving primarily atomic motion of cations against their oxygen neighbors. Consequently, these modes are very sensitive to the cationic local environment in the host matrix. Fig. 5 shows the FTIR spectra of glycine-nitrate synthesized

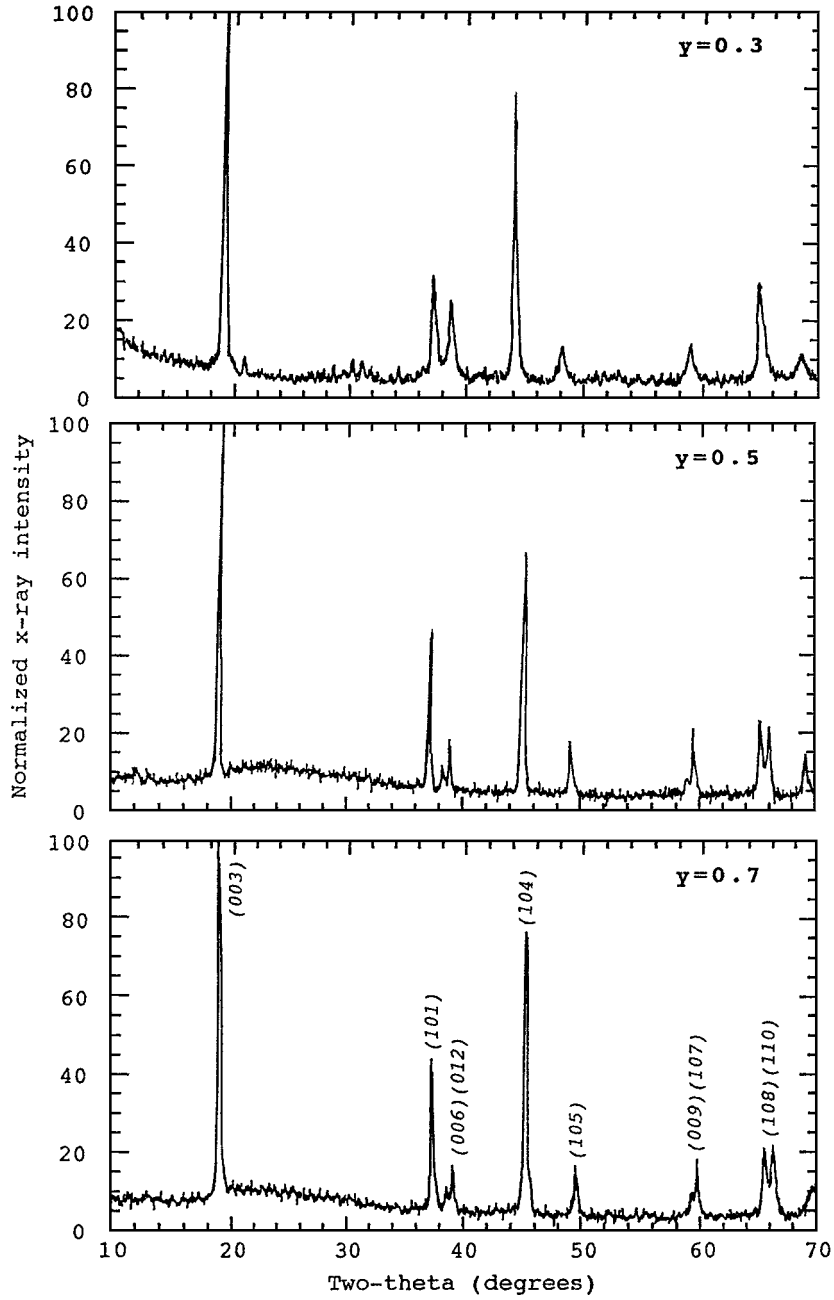

Figure 3 Observed x-ray diffraction patterns of microcrystalline $LiNi_{1-y}Co_yO_2$ ($0.3 \leq y \leq 0.7$) powders calcined at 600°C and synthesized by the glycine-assited combustion method. XRD peaks were indexed assuming the $R\bar{3}m$ symmetry (hex.).

$LiNi_{1-y}Co_yO_2$ samples fired at 600°C for 5 hours. The FTIR absorption spectra display features which can be divided into two parts. (i) The high-wavenumber region of strong absorption corresponds to the broad rock-salt band which has broken into several distinct components at ca. 400–600 cm^{-1}, and (ii) the low-wavenumber region in which an isolated strong band is centered at ca. 240–260 cm^{-1}. The frequency of the vibrational modes and the analysis of the spectroscopic data of $LiNi_{1-y}Co_yO_2$ are summarized in Table II.

Layered oxides $LiMO_2$ possess a crystal structure consisting of alternating layers of trigonally distorted LiO_6 and MO_6 octahedra sharing edges. It has been shown that $LiNi_{1-y}Co_yO_2$ is a solid solution of $LiMO_2$ (M = Ni, Co) compounds and that stoichiometric compounds belong to crystallographic $R\bar{3}m$ space group. The transition-metal cations (i.e. cobalt and nickel) and the lithium ions are located at Wyckloff sites 3(b) and 3(a), respectively, in a cubic close-packed oxygen array. The Li^+ and Co^{III}/Ni^{III} ions are ordered along the (111) direction of the rock-salt cubic lattice leading to a two-dimensional structure. The IR modes of crystalline $LiNi_{1-y}Co_yO_2$ can be predicted by factor group analysis with a Bravais cell which contains

TABLE II Wavenumbers (in cm^{-1}) and assignments of the IR-active modes of the layered $LiNi_{1-y}Co_yO_2$ compounds calcined at 600°C as a function of cobalt content

	Cobalt content (y)			
Mode	0.3	0.5	0.7	Assignment
ν_1	243	245	250	$\nu(LiO_6)$
ν_2	355/410	416	430	$\delta(MO_6)$
ν_3	510	527	534	$\delta(MO_6)$
ν_2	574	580	589	$\nu(MO_6)$

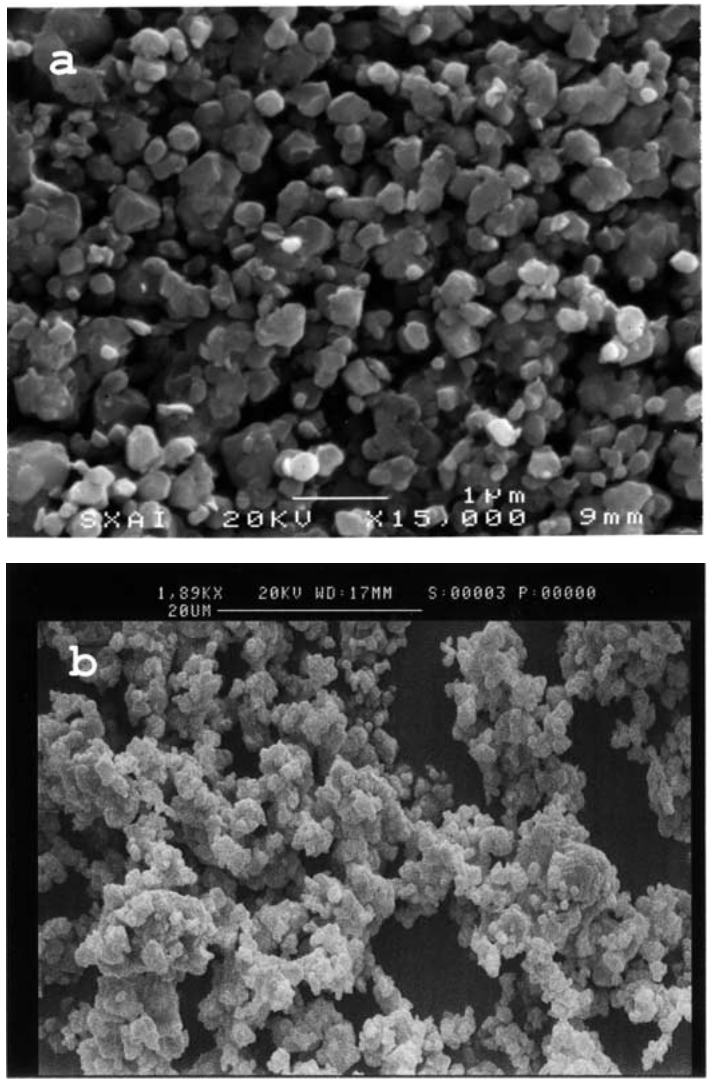

Figure 4 Typical SEM micrographs of (a) $LiNi_{0.3}Co_{0.7}O_2$ and (b) $LiNi_{0.5}Co_{0.5}O_2$ samples calcined at 600°C.

one molecule ($Z = 1$). The group factor analysis of the D^5_{3d} spectroscopic symmetry yields four infrared-active modes [26]. Because FTIR spectroscopy is capable of probing directly the surrounding environment of the cation, we have studied the local environment of lithium ions in $LiMO_2$ materials [27–29]. It has been also demonstrated that the IR resonant frequencies of alkali metal cations in their octahedral interstices in inorganic oxides are located in the frequency range 200–300 cm^{-1} [30]. Our recent work on transition-metal substitution in $LiMO_2$ compounds has shown that vibrational mode component of the LiO_6 octahedra appears invariably around 250 cm^{-1} [31]. Thus, the IR resonant frequency of LiO_6 groups appears at 269 and 234 cm^{-1} in the $LiCoO_2$ and $LiNiO_2$ layered structures ($R\bar{3}m$ space group), respectively. As far as the low-wavenumber peak is concerned, the isotopic Li replacement in $LiMO_2$ has proven that this IR band between 200–300 cm^{-1} is associated to vibration of a relatively isolated LiO_6 octahedron [32].

Thus, the IR absorption bands of $LiNi_{1-y}Co_yO_2$ microcrystalline powders are attributed as follows. The band situated at 245 cm^{-1} is assigned with confidence to an asymmetric stretching vibration of the Li^+ ion with O^{2-} near neighbors in $LiNi_{0.5}Co_{0.5}O_2$. However, a small mixing of Li-O stretching and O-M-O bending motion is present in the low-wavenumber peak. The high-frequency band of the FTIR absorption spectrum of $LiNi_{0.5}Co_{0.5}O_2$ located at ca. 580 cm^{-1} is attributed to the asymmetric stretching mode of MO_6 group, whereas the low-frequency bands at ca. 416 and 527 cm^{-1} are assigned to the bending modes of O-M-O chemical bonds.

FTIR measurements confirm XRD data showing the growth of structurally well-formed $LiNi_{0.3}Co_{0.7}O_2$ layered phase. However, we got additional information on the lattice structure, especially on the distribution of the transition metal in the (Ni, Co)O_2 slabs. The shape of the FTIR spectra of the cobalt-rich products (Fig. 5) shows the predominance of the stretching modes. The frequency shift of both the IR bending and stretching modes are due to the change in the volume of the unit cell and, of course, to the modification of the covalency of the $(Ni_{1-y}Co_y)O_2$ layers upon Co substitution. The frequency shift of the LiO_6 mode has two origins: (i) the slight expansion of the interslab distance (c_{hex} cell parameter) in $LiNi_{1-y}Co_yO_2$ samples and (ii) the small mixing of Li-O stretching and O-M-O bending motion present in the low-wavenumber peak.

The broadening of the high-wavenumber IR bands may be related with inhomogeneous Ni/Co distribution, variation in the cation-anion bond lengths,

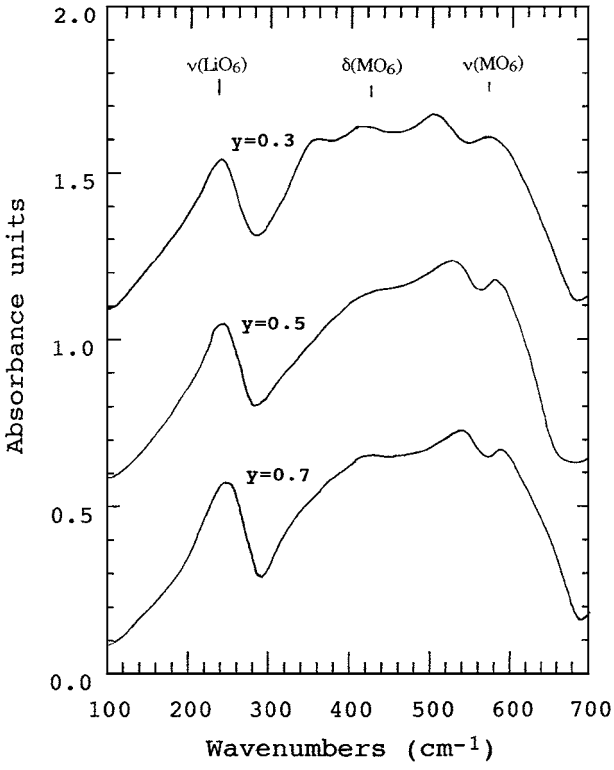

Figure 5 Typical room temperature FTIR absorption spectra of $LiNi_{1-y}Co_yO_2$ ($0.3 \leq y \leq 0.7$) samples prepared by the low-temperature synthesis and calcined at 600°C.

and/or polyhedral distortion occurring in nickel-rich $LiNi_{0.7}Co_{0.3}O_2$. It has been reported that the local distortion increases with the decrease of the cobalt concentration in the solid solution [33]. Recording ^7Li NMR spectra of $LiNi_{1-y}Co_yO_2$ compounds, Delmas *et al.* [34, 35] have detected slight deviations from a homogeneous Ni/Co distribution and cobalt segregation in the $LiNi_{1-y}Co_yO_2$ solid solution. It seems that the predominance of the bands in medium-range frequency of the IR spectrum of the product with $y = 0.3$ is due to a local disorder in the (Ni, Co)O_2 slabs, i.e., inhomogeneous Ni/Co distribution. These results show that FTIR of $LiNi_{0.7}Co_{0.3}O_2$ materials permits the accurate detection of short scale heterogeneities complementing the x-ray diffraction analysis which only provides information on the long-range structure.

3.4. Electrochemical studies

Electrochemical studies in lithium cells were carried out to compare the performance of low-temperature electrodes prepared by glycine-assisted combustion method. Electrochemical properties were examined in lithium-containing test cells employing a non-aqueous electrolyte medium. The electrodes are separated by a porous membrane soaked in an electrolyte of 1*M* $LiPF_6$ in 1 : 1 (v/v) mixture of EC-DMC. The voltage-composition curves of the electrochemical cells using combustion-synthesized cathodes are given in Fig. 6. The Li//$LiNi_{1-y}Co_yO_2$ cells were charged and discharged at current densities of 0.1 mA/cm^2, while the voltage was monitored between 2.5 and 4.0 V using the galvanostatic mode of the MacPile battery tester. These experiments have been carried out at low rates to emphasize the relationship between structure and electrochemistry. Fig. 6 represents the evolution of the cell potential after each period of relaxation. So, these charge-discharge curves correspond to the open-circuit voltage.

In the potential domain 3.0–4.0 V, the charge-discharge curves correspond to the voltage profiles characteristic of the $Li_xNi_{1-y}Co_yO_2$ cathode materials associated with lithium occupation of octahedral sites, in agreement with previous works [7, 13]. However, low-temperature synthesized $Li_xNi_{1-y}Co_yO_2$ cathode materials show a lower potential for lithium deintercalation-intercalation than the materials prepared at high temperature, i.e., 800°C [36]. Similar

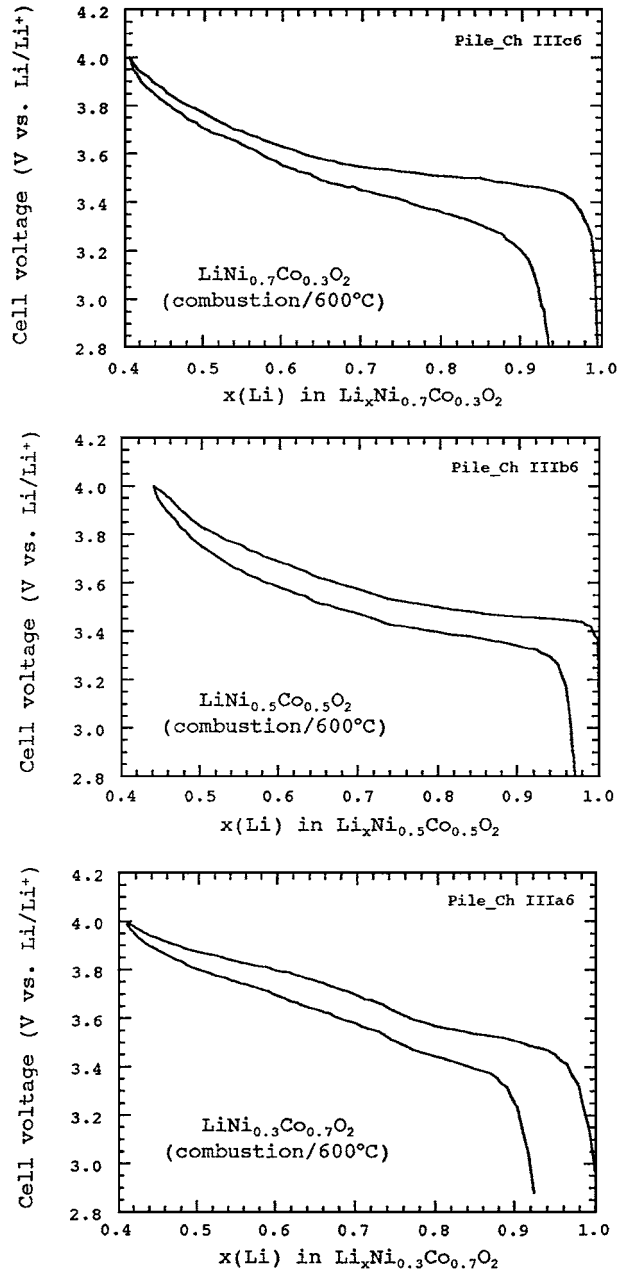

Figure 6 Typical charge-discharge characteristics of Li//$LiNi_{1-y}Co_yO_2$ non-aqueous cell employing the electrolyte of composition 1*M* $LiPF_6$ in EC-DMC (1 : 1) at room temperature. Charge and discharge were obtained at current density 0.1 mA/cm^2. Cathode materials prepared by the glycine-assisted method were calcined at 600°C. Data were taken at the end of each relaxation period.

behavior is also observed in the present investigation. The voltage profile of the cell Li//$LiNi_{0.7}Co_{0.3}O_2$ exhibits a potential slightly lower than for other synthesized glycine-assisted compounds. This is due to the different crystallographic texture and morphology of these two materials. It should be remarked that the fully intercalated phase is not recovered during the first discharge. This could be probably assigned to a kinetic problem especially as the phase $Li_xNi_{0.7}Co_{0.3}O_2$ is a poor electronic conductor. However, the polarization during both charge and discharge is almost similar in all cells. These studies also demonstrate that, obviously, the positive electrode yields capacities around 145 mAh/g when charged to a cut-off voltage of 4.2 V compared to the theoretical value of 164 mAh/g (corresponding to $\Delta x = 0.6$). The improved performance of the Li//$LiNi_{0.5}Co_{0.5}O_2$ cell is evident (Fig. 6) from the following factors: (i) the rate at which the capacity is lost on cycling is reduced and (ii) the potential is superior in the entire length of charge-discharge.

The shape of the charge-discharge curves shows a good reversibility during the first cycle. In the composition domain $0.4 \leq x \leq 1.0$, the voltage charge profile of the Li//$Li_xNi_{0.7}Co_{0.3}O_2$ cell exhibits an increase of the potential followed by a plateau at ca. 3.5 V. For $x < 0.5$, the high voltage limit imposed in the experiments is rapidly reached. From the variation of the cell potential for the complete cell (Fig. 6), one can distinguish the presence of two regions during the lithium insertion-extraction process. The voltage profile displays two flat domains separated by an intermediate domain characterized by a potential jump from 3.5 to 3.8 V around the composition $Li_{0.7}Ni_{0.7}Co_{0.3}O_2$ during the first charge. The first stage (I), near 3.5 V, is assigned to oxidation of Ni^{3+} ions. In the initial composition region ($1.0 \geq x \geq 0.7$), the electrochemical charge curve (deintercalation process) is almost similar to that of the nickelate compound, while at $x < 0.7$ the profile is very close to that of the Li//Li_xCoO_2 cell. Thus, the second stage (II), near 3.8 V, is attributed to oxidation of Co^{3+} ions. These evolutions come from the prior oxidation of Ni^{III} ions before the cobalt ions. These results are in good accordance with the work reported by Delmas *et al.* [13]. They have demonstrated that, for cobalt-rich phases, the Ni^{III} ions are preferentially oxidized to the tetravalent state in comparison with the Co^{III} ions.

The lithium extraction/insertion reactions in regions I and II proceed in a $Li_xNi_{0.3}Co_{0.7}O_2$ matrix having a rhombohedral symmetry. Considering the fully charge state (at 4 V, $x = 0.4$), the classical reaction in a Li//$LiNi_{0.3}Co_{0.7}O_2$ intercalation cell can be written as

$$\square_{0.6}Li_{0.4}\left[Ni^{4+}_{0.3}Co^{4+}_{0.3}Co^{3+}_{0.4}\right]O_2 + 0.6Li^+ + 0.6e^- \longleftrightarrow LiNi_{0.3}Co_{0.7}O_2, \quad (2)$$

which normally lies in between the voltage 4 and 3 V. The layered $LiNi_{0.3}Co_{0.7}O_2$ framework provides a two-dimensional interstitial space for rapid lithium intercalation and deintercalation. It is believed that the *c*-axis of the layered materials expands rapidly on delithiation due to a decrease of the electrostatic binding energy of the lithium-depleted layers [7]. As a concluding remark, it can be pointed out that low-temperature cathode materials exhibit acceptable electrochemical capacity with lower oxidation potential. These compounds are candidates to treat problems due to nickel dioxide formation and electrolyte degradation. This shows the advantage of the wet-chemical synthesis method for $Li_xNi_{1-y}Co_yO_2$ preparation, since materials having similar properties can be elaborated in shorter time to reduce the cost of cathode materials. The electrochemical properties of $Li_xNi_{1-y}Co_yO_2$ cathode materials are presently being studied for long term cycling.

4. Conclusion

This work have shown that $Li_xNi_{1-y}Co_yO_2$ ($0.3 \leq y \leq 0.7$) single phases were grown at low temperature using the aqueous glycine-nitrate combustion process. The low-temperature method, in which glycine acts such as a fuel, provides submicron-sized particles which are adequate for fast lithium intercalation-deintercalation reactions occurring in rechargeable lithium cells. The use of solution processing leads to molecular level mixing and highly uniform materials. The low-temperature technique adopted for the synthesis of $Li_xNi_{1-y}Co_yO_2$ cathode materials has yielded particles with grain size in the range 600–800 nm which favor good electrochemical performance. However, the nickel-rich compound has a structure exhibiting a departure from the 2D lattice and contains some impurities. It seems that combustion method does not work well for $Li_xNi_{1-y}Co_yO_2$ materials with $y \geq 0.7$. The charge-discharge voltage profiles of Li//$Li_xNi_{1-y}Co_yO_2$ cells show evolutions which come from the prior oxidation of Ni^{III} ions before the cobalt ions. These studies also demonstrated that the combustion synthesized-cathodes yield capacities in the range 120–135 mAh/g when discharged to a cut-off voltage of 2.8 V ($1.0 \geq x \geq 0.4$). The improved performance of the Li//$Li_xNi_{0.5}Co_{0.5}O_2$ cell using cathode prepared by the aminoacetic acid-assisted method is evident from the rate at which the capacity is lost on cycling is reduced and the potential superior occurring in the entire length of charge-discharge.

References

1. K. MIZUSHIMA, P. C. JONES and J. B. GOODENOUGH, *Mater. Res. Bull.* **15** (1980) 763.
2. T. NAGAURA, Paper presented at the 4th Intl. Rechargeable Battery Seminar, Deerfield Beach, FL (March 1990).
3. J. R. DAHN, U. VON SACKEN and R. FONG, Primary and Secondary Batteries Symposium, 178th Electrochem. Soc. Meeting, Seattle, WA (Oct. 14–10, 1990).
4. Y. NISHI, H. AZUMA and A. OMARU, US Patent no. 4,959,281 (1990).
5. T. NAGAURA and K. TOZAWA, *Prog. Batt. Solar Cells* **9** (1990) 209.
6. M. G. S. R. THOMAS, W. I. F. DAVID, J. B. GOODENOUGH and P. GROVES, *Mat. Res. Bull.* **20** (1985) 1137.
7. R. J. GUMMOW and M. M. TACKERAY, *Solid State Ionics* **53–56** (1992) 681.
8. C. DELMAS and I. SAADOUNE, *ibid.* **53–56** (1992) 370.

9. T. OHZUKU, A. UEDA, M. NAGAYAMA, Y. IWAKOSHI and H. KOMORI, *Electrochim. Acta* **38** (1993) 1159.
10. E. ZHECHEVA and R. STOYANOVA, *Solid State Ionics* **66** (1993) 143.
11. A. ROUGIER, I. SAADOUNE, P. GRAVEREAU, P. WILLMANN and C. DELMAS, *ibid.* **90** (1996) 63.
12. C. DELMAS, I. SAADOUNE and A. ROUGIER, *J. Power Sources* **43/44** (1993) 595.
13. I. SAADOUNE and C. DELMAS, *J. Mater. Chem.* **6** (1996) 193.
14. P. BARBOUX, J. M. TARASCON and F. K. SHOKOOHI, *J. Solid State Chem.* **94** (1991) 185.
15. E. ROSSEN, J. N. REIMERS and J. R. DAHN, *Solid State Ionics* **62** (1993) 53.
16. B. GARCIA, P. BARBOUX, F. RIBOT, A. KAHN-HARARI, L. MAZEROLLES and N. BAFFIER, *ibid.* **80** (1995) 111.
17. I.-H. OH, S.-A. HONG and Y.-K. SUN, *J. Mater. Sci.* **32** (1997) 3177.
18. S. R. S. PRABAHARAN, M. S. MICHAEL, T. P. KUMAR, A. MANI, K. ATHINARAYANSWAMY and R. GANGADHARAN, *J. Mater. Chem.* **5** (1995) 1035.
19. J. P. PERERA-RAMOS, *J. Power Sources* **54** (1995) 120.
20. C. J. BRINKER and G. W. SCHERER, "Sol-Gel Science: The Physics and Chemistry of Sol-Gel Processing" (Academic Press, London, 1990).
21. H. TAGUCHI, H. YOSHIOKA, D. MATSUDA and M. NAGAO, *J. Solid State Chem.* **104** (1993) 460.
22. S. KUMAR SAHA, A. PATHAK and P. PRAMANIK, *J. Mater. Sci. Lett.* **14** (1995) 35.
23. G. G. AMATUCCI, N. PEREIRA, T. ZHENG, I. PLITZ and J. M. TARASCON, *J. Power Sources* **81/82** (1999) 39.
24. J. MORALES, C. PEREZ-VICENTE and J. L. TIRADO, *Mater. Res. Bull.* **25** (1990) 623.
25. J. R. DAHN, U. VON SACKEN and C. A. MICHAEL, *Solid State Ionics* **44** (1990) 87.
26. R. K. MOORE and W. B. WHITE, *J. Amer. Ceram. Soc.* **53** (1970) 679.
27. C. JULIEN, A. ROUGIER and G. A. NAZRI, *Mater. Res. Soc. Symp. Proc.* **453** (1997) 647.
28. A. ROUGIER, G. A. NAZRI and C. JULIEN, *Ionics* **3** (1997) 170.
29. M. NAZRI, D. CURTIS, B. YEBKA, G. A. NAZRI and C. JULIEN, Extended Abstracts of 193th Meeting of The Electrochem. Soc., San Diego, CA (May 3–8, 1998).
30. G. J. EXARHOS and W. N. RISEN, *Solid State Commun.* **11** (1970) 755.
31. G. A. NAZRI, A. ROUGIER and K. F. KIA, *Mater. Res. Soc. Symp. Proc.* **453** (1997) 635.
32. P. TARTE and J. PREUDHOMME, *Spectrochim. Acta* **26A** (1970) 747.
33. C. JULIEN, M. MASSOT, C. PEREZ-VICENTE, E. HARO-PONIATOWSKI, G. A. NAZRI and A. ROUGIER, *Mater. Res. Soc. Symp. Proc.* **496** (1998) 415.
34. C. MARICHAL, J. HIRSCHINGER, P. GRANGER, M. MENETRIER, A. ROUGIER and C. DELMAS, *Inorg. Chem.* **34** (1995) 1773.
35. M. MENETRIER, A. ROUGIER and C. DELMAS, *Solid State Commun.* **90** (1994) 439.
36. D. CAURANT, N. BAFFIER, B. GARCIA and J. P. PEREIRA-RAMOS, *Solid State Ionics* **91** (1996) 45.

Received 21 December 1999
and accepted 21 December 2001